Dynamic and static position control of optical feedback solitons

Björn Gütlich,[a] Holger Zimmermann, Carsten Cleff, and Cornelia Denz[b]
Institut für Angewandte Physik, and Center for Nonlinear Science,
Westfälische Wilhelms Unisversität Münster, Corrensstraße 2-4, 48149 Münster, Germany

(Received 12 February 2007; accepted 9 July 2007; published online 28 September 2007)

We report on the experimental implementation of an external control for optical feedback solitons using incoherent spatial intensity distributions in a liquid crystal light valve (LCLV) optical single feedback system. The external control provides excellent experimental possibilities for static and dynamic control of the lateral positions of the optical feedback solitons which will be demonstrated. Particularly, the influence of different gradients onto the drift motion of spatial solitons is experimentally investigated in detail. In agreement with theoretical predictions, the drift velocity of the soliton increases according to the steepness of the gradient. Additionally, a completely incoherent addressing scheme including creation and erasure of feedback solitons is demonstrated for the LCLV setup. © *2007 American Institute of Physics*. [DOI: 10.1063/1.2767405]

Spontaneous interactions and spatial inhomogeneities are challenges for potential applications of dissipative spatial optical solitons in the context of all optical information processing. The attractiveness of dissipative solitons for applications is justified by the robustness of their spatial structure against perturbations and their binary features, which motivate their interpretation as the natural bit of nonlinear optics. To address the challenges mentioned above, the implementation of control schemes for dissipative optical solitons is necessary. In this contribution we will discuss the successful experimental realization of a static and dynamic position control for spatial optical feedback solitons by means of an external amplitude control scheme. The method also enables a previously inaccessible complete addressing scheme allowing for incoherent erasure of individual feedback solitons.

I. SPATIAL OPTICAL FEEDBACK SOLITONS

Spatial optical solitons are nonlinear objects which preserve their shape during propagation. For the existence of these self-preserving spatial structures in an optical system, diffraction, which causes a broadening of optical beams, needs to be balanced by a self-focusing nonlinearity. These spatial optical solitons exist in different configurations. In the most basic configuration a spatial soliton forms while a confined light beam propagates through a saturable optical nonlinear bulk medium.[1–4] Other prominent configurations, which allow for the formation of spatial optical solitons, besides the balance between optical nonlinearity and diffraction, require a balance between gain and loss far from thermodynamical equilibrium as well as an inherent feedback mechanism. These so-called dissipative solitons[5–17] share many features with propagating solitons, are for example found in optical resonators, and thus are often denoted as "cavity solitons."[5–12] Even a semicavity with a single feedback mirror is sufficient to support spatial dissipative solitons, because the single mirror already provides the feedback mechanism required.

Emerging from investigations on the spontaneous formation of spatial optical pattern,[18–22] single feedback systems, e.g., with atomic vapors and liquid crystal light valves as optical nonlinearities, are well-known to support spatial optical solitons.[22–26] In these systems the nonlinear optical medium can be considered to be optically thin, thus allowing for a separated treatment of the effects induced by the nonlinearity and the linear diffraction, which in turn simplifies experimental and theoretical treatment. In the following we will refer to spatial solitons existing in such a single feedback configuration as "feedback solitons."[5]

The features of cavity and feedback solitons are astonishingly similar. Both can be written, stored, readout, and erased, and thus can be interpreted as natural bits of nonlinear optical systems and may open ways for new kinds of parallel all-optical information processing schemes.[27] As potential applications for feedback and cavity solitons, the implementation of flexible all-optical memories, shift registers as well as all-optical switching and routing of optical data have been suggested.[27–29] Due to the strong similarities between feedback and cavity solitons, observations made with feedback solitons can excellently be transferred to cavity solitons and vice versa. For investigations of the fundamental experimental behavior of this class of solitons, single feedback systems have become a commonly used model system. Among the advantages of feedback systems investigated in experiment are high sensitivities of the nonlinearity, comparatively small spatial inhomogeneities, and response times, which make the experimental monitoring of the spatial and temporal dynamics of the solitons much more accessible in experiment. Fast response times as well as other technological aspects however make semiconductor devices the more likely solution for future application.[5]

The name single feedback derives from the fact, that the optical wave front travels around the system once only. A single feedback system works in the following way: a plane

[a]Electronic mail: guetlich@uni-muenster.de
[b]Electronic mail: denz@uni-muenster.de

pump wave is spatially (phase-) modulated by passing a nonlinear medium. The modulated wave propagates in free space over a certain distance while it experiences diffraction. The resulting wave is then fed back to the nonlinear material. During propagation, diffraction causes the transformation of small intrinsic modulations in the transverse phase profile into spatial amplitude modulations due to the well-known Talbot effect.[19] The corresponding intensity profile then interacts with the plane pump wave via the nonlinear material.

A crucial prerequisite for potential applications of feedback solitons is a complete and robust addressing scheme for the solitons, including writing, erasure, and reliable storage of individual solitons. Yet, addressing and reliable storage of feedback- and cavity solitons is obstructed by influences of spatial inhomogeneities and spontaneous interaction behavior of the solitons, which for examples result in spontaneous motions and spontaneous pinning. This spontaneous behavior primarily is caused by phase gradients present in the optical feedback wave.[8,24,30,31] Therefore modifications of these phase gradients, as we will experimentally show in the following, are the main key for controlling spatial feedback solitons.

In theoretical investigations it has been observed that feedback solitons drift along these phase gradients and they finally accumulate at the local extrema of the gradient.[32,33] The drifting velocity is predicted to relate linearly with the steepness of the gradient.[34,35] Two main sources of these phase gradients can be identified. One source are global phase gradients, which can either be induced by global influences such as spatial inhomogeneities of the system, for example, caused by nonuniform spatial response of the optical nonlinearity. Local extrema in such global phase gradients can result in the pinning of feedback solitons to spontaneous favorite trapping positions.[29] The second source for phase gradients are the feedback solitons themselves. Feedback solitons are accompanied by oscillating tails, which can be interpreted as self-diffraction rings with a phase profile.[30,31] As a consequence, the oscillating tails of feedback solitons induce interactions of neighboring feedback solitons. Due to the resulting mutual interaction, locking of feedback solitons at characteristic interaction distances has been reported.[23,29] The resulting phase gradient present in the system therefore can be interpreted as a potential, which determines the spontaneous motion of feedback solitons as well as their final equilibrium state. Therefore, suitable control schemes allowing for static and dynamic lateral positioning are required to control the spontaneous motions of feedback solitons.

In this contribution we will report on the experimental implementation of an external amplitude control, which provides a position control needed for reliable and robust addressing of feedback solitons. As a model system for our investigations we choose a single feedback experiment, which uses a liquid crystal light valve (LCLV) as nonlinearity. Apart from the reasons mentioned above, the LCLV single feedback setup is particularly well suited as a model system for our investigation, because it can be operated at comparatively small intensities and provides very large aspect ratios allowing for the addressing of large arrays of solitons. The results obtained in our model system can be transferred to other systems due to the similarities between feedback and cavity solitons. In Sec. II we will review the LCLV single feedback mirror system and explain the appearance of feedback solitons in this system. In Sec. III we will then discuss the effect of external control onto these feedback solitons. We will show the (to our knowledge) first time implementation of a static and dynamic position control of feedback solitons by an external amplitude control. Furthermore, a complete robust and incoherent addressing scheme including writing and incoherent erasure of feedback solitons is demonstrated. This method improves a previously realized, less robust addressing scheme which uses coherent addressing beams and which thus exhibits extreme sensitivity against perturbations.[24] Based on the pioneering experiments on the control of feedback solitons with incoherent intensity distributions we will go on to investigate the influence of a gradient induced drift motion in a cone gradient with increasing steepness. Thus, not only the final equilibrium positions of the feedback solitons, but also the dynamic response of feedback solitons to external amplitude control is investigated. Furthermore, the control scheme is extended to more complex control geometries in investigating the interaction of feedback solitons with a hexagonal gradient using different hexagon wavelengths.

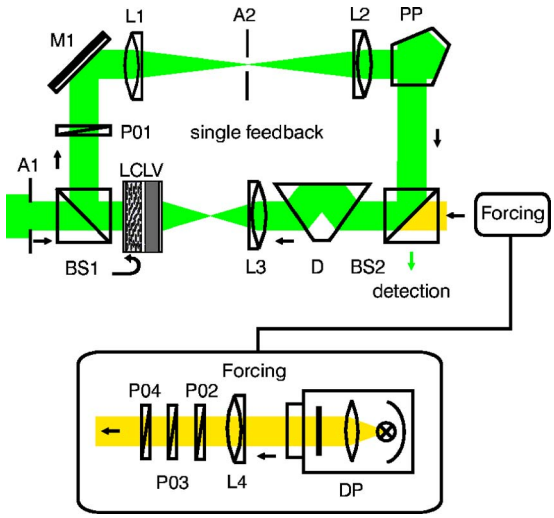

FIG. 1. (Color online) Schematic setup of the LCLV single feedback system including external amplitude control. Concept of the external amplitude control (forcing). A digital projector DP images a incoherent intensity distribution, which is used as forcing, onto the LCLV. The polarizers PO2, PO3, and PO4 adjust forcing intensity and polarization state.

II. FEEDBACK SOLITONS IN THE LCLV SINGLE FEEDBACK SYSTEM

A. LCLV single feedback system: Experimental setup and theoretical model

In the system under investigation, a liquid crystal light valve (LCLV) which acts as an optically addressable spatial light modulator, is used as optical nonlinearity. A schematic setup of the LCLV single feedback system is shown in Fig. 1.

The LCLV can be treated as a composition of two functional elements, a read and a write side.[20] The read side consists of a nematic liquid crystal layer (LC) in planar

alignment, and a dielectric mirror. The write side consists of a photo conductor. Both readout and write side are embedded between transparent electrodes. For operation, an ac bias voltage is externally applied via the transparent electrodes. A light wave incident at the liquid crystal readout side is reflected at the internal mirror and experiences a phase shift according to the spatial refractive index distribution of the liquid crystal layer. At the same time also the polarization state becomes modulated depending on the angle Ψ between the incident linearly polarized optical wave and the optical axis of the liquid crystal. The light intensity incident at the photoconductive write side increases the capacitive conductance of the photoconductor and thus locally increases the voltage drop over the liquid crystal layer. As a consequence, the liquid crystal layer changes its refractive index. This way a spatial intensity distribution incident at the LCLV's write side is transformed into a modulation of the refractive index of the readout layer.

Due to the optical properties of its liquid crystal layer, the LCLV typically acts as a defocusing nonlinearity. A focusing nonlinearity however can also be created using a system inherent symmetry of the optical feedback.[19] This will be discussed in detail after the feedback loop has been introduced.

The phase shift induced by the LCLV nonlinearity can be written as[20]

$$\tau\frac{\partial}{\partial t}\Phi - l^2\nabla_\perp^2\Phi + \Phi = \Phi_{\max}\{1 - \tanh^2(S(I_w, U_{\text{ext}}))\},$$
$$S(I_w, U_{\text{ext}}) = S_0\frac{\kappa_1 I_w + 1}{\kappa_2 I_w + 1}\frac{U_{\text{ext}} - U_{\text{th}}}{U_0}. \tag{1}$$

In this equation, $\tau \approx 50$ ms is the effective response time of the LCLV and $l = 30$ μm the effective diffusion length which limits the transversal resolution of the LCLV. I_w is the intensity incident at the photoconduction write side, U_{ext} the externally applied ac voltage, $\Phi_{\max}$, S_0, κ_1, κ_2, U_{th}, and U_0 are device specific parameters.

After modulation of its phase profile according to Eq. (1) and internal reflection, the incident readout wave from a cw laser ($\lambda = 532$ nm) is coupled into the feedback loop by a beamsplitter. Within the feedback loop it propagates in free space over the distance L, passes a polarizer (P01) and is then imaged to the LCLV's photoconductive write side by different optical components like lenses (L), mirrors (M), a penta prism (P), and a dove prism (D). The dove prism is used in the experimental setup to balance rotational misalignments which may be induced by the mirrors, while the penta prism (P) ensures an even number of reflections in the setup. The polarizer (P01) transmits at an angle of $-\Psi$ with respect to the optical axis of the liquid crystal. At beamsplitter BS2, a fraction of light is extracted to record the optical near and far field (Fourier transform) with a CCD camera. The resulting intensity distribution I_w at the photoconductive write side can be written as

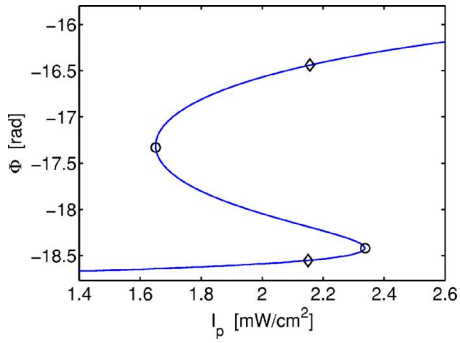

FIG. 2. (Color online) Exemplary bistability curve of the phase ϕ in relation to the pump intensity I_p. In the ranges between ($\diamond$) and ($\bigcirc$) patterned system states are observed. Feedback solitons spontaneously form in the region where a uniform lower state coexists with a patterned upper state.

$$I_w = |e^{-i(L/2k)\nabla_\perp^2}\{(Be^{-i\Phi} + C)\}|^2 I_p, \tag{2}$$

where L is the propagation length, k is the wave vector of the laser light, and $e^{-i(L/2k)\nabla_\perp^2}$ is the propagation operator. The amplitude factors $B = \cos^2\Psi$ and $C = \sin^2\Psi$ describe the influence of the polarization. For $B = 1$ and $C = 0$ and thus $\Psi = 0$, a phase only modulation is introduced. I_p is the intensity of the linearly polarized pump wave. To enable the formation of robust optical feedback solitons, a self-focusing nonlinearity is needed. In order to create a self-focusing nonlinearity—the LCLV itself acts as mentioned above self-defocusing—a symmetry in the model is used. In replacing a positive propagation length L with a virtual propagation length $-L$ the characteristics of the nonlinearity switches from defocusing to focusing.[19] This configuration is realized by imaging a virtual mirror plane in front of the LCLV's readout side to the photoconductive side. In the experiments reported here a propagation length of $L = -15$ cm is used.

If the pump intensity which acts as the stress parameter of the LCLV single feedback system is increased, the homogenous solution of the planar wave becomes modulationally unstable against spatial perturbations above a threshold intensity. The modulation instability[20] results in the spontaneous formation of spatial optical structures such as hexagons, stripes, inverted hexagons, and spatio-temporally complex system states.[20,36] In specific parameter regimes, the formation of optical feedback solitons is observed in this system.[24,25,37]

For the creation of bright feedback solitons in the LCLV single feedback system, a bistability between a uniform dark state and a bright patterned state is experimentally essential. In a more general context, however, bistability between homogeneous or patterned system states and any combination of these allow for the existence of optical feedback solitons. If the system runs in polarization mode (i.e., $\Psi \neq 0$), such a bistability can be induced. The feedback solitons in this case represent a solution of the system, which connects the stationary uniform dark solution with the patterned bright solution (cf. Fig. 2) The largest parameter range of bistability is expected to be at $\Psi = 45°$. Therefore, the system is operated near this value. For a more detailed discussion on the parameter ranges for bistability and the range of feedback solitons existence please refer to Ref. 37.

B. Dynamics of feedback solitons

As discussed above, phase gradients present in the optical feedback beam influence the motion of optical feedback solitons. In the LCLV single feedback system both the influence of global gradients as well as mutual interactions of feedback solitons have been observed.[24] After the writing of feedback solitons and transient behavior, typically equilibrium states in which the feedback solitons come to rest at spontaneous trapping positions are observed.[29] The transient interaction behavior induced by the local environment of the feedback solitons and by the LCLV feedback solitons themselves before they settle into their final spontaneous equilibrium state however includes spontaneous motions, pinning to favorite trapping positions, locking at characteristic interaction distance as well as merging of neighboring feedback solitons and spontaneous disappearance of feedback solitons.[29] In the following we will explore how external amplitude control enables the suppression of these unwanted spontaneous dynamics and we will study how the lateral static and dynamic positions of feedback solitons and the addressing behavior including writing and erasing can be controlled in a reliable and robust manner.

III. EXTERNAL CONTROL OF FEEDBACK SOLITONS

Previously, control of feedback solitons has been implemented mainly using Fourier control techniques.[29,37–40] However, Fourier control does not allow for an absolute position control of individual feedback solitons required for implementation of a robust addressing. The challenge therefore is to establish an all-optical real-space control which does not destroy the existence of the feedback solitons while conserving the essential spatial flexibility of the solitons in the system and which counterbalances the spontaneous behavior of feedback solitons and system inhomogeneities. For this purpose, the implementation of external phase or amplitude control in real space has been suggested alternatively.[28,41–44] Here, we will experimentally use an additional spatial intensity distribution for the external control of the system. The external amplitude control imposes a stimulus to the nonlinear optical feedback system, which we will in the following name "forcing" in analogy to the forcing of one-dimensional temporal oscillators.[45,46] External amplitude control must be considered as an invasive control method since it changes the system state of the control system in any case. Due the invasive character of forcing, the response of the system to system solutions not inherently present in the system can be investigated. Furthermore, the adjustment of the control strength is of crucial importance. The strength of the external control must be adjusted such that it does not absolutely dominate the system behavior by itself. In our particular example, the forcing strength must be strong enough to influence the behavior of feedback solitons, but at the same time must not destroy the ability of the system to support feedback solitons. Previously, such an external control scheme has successfully been implemented in the LCLV single mirror feedback system for the forcing of a spatial pattern.[45,46]

Experimentally forcing is realized by projecting an incoherent spatial intensity I_f to the LCLV's photoconductive write side (cf. Fig. 1). The spatial distribution of the static or dynamic forcing signal is designed at a computer. The forcing intensity distribution is created by a LCD-data projector. Lens (L7) projects the intensity distribution of the external amplitude control into the feedback system. The forcing strength can be controlled with the help of three polarizers. The first polarizer PO2 selects the green fraction of the data-projector's RGB signal, polarizer PO4 determines the polarization state of the forcing input, while polarizer PO3 is rotated to adjust the external control strength.

To model the influence the forcing I_w in Eq. (2) simply must be replaced by the total intensity

$$I_{\mathrm{tot}}(x,y,t) = I_w(x,y,t) + I_f(x,y,t). \tag{3}$$

The effect of the forcing onto the feedback system is twofold. First, the offset intensity acts locally similarly to the external bias voltage [U_{ext} in Eq. (1)] and, i.e., the operation point of the nonlinearity is shifted locally.[20] Second, the additional intensity distribution I_f induces an offset in the nonlinearly induced phase distribution ϕ of the feedback wave. Thus, an additional phase modulation of the feedback wave can be achieved.[43]

A. Static position control

In our first approach to statically control the transverse positions of feedback solitons we used a chessboard pattern with bright and dark quadratic fields as a forcing signal.[40] In these first experiments we showed that the forcing method succeeds in controlling the absolute positions of feedback solitons. However, the quadratic shape of the chessboard fields leaves the feedback solitons a certain range of space. Thus, a precise lateral positioning in some areas has not yet been achieved. Here we report on a altered version of our method, which allows for a more precise lateral positioning. For this purpose, the forcing intensity distribution was altered. Instead of quadratically shaped chessboard fields, Gaussian shaped peaks with a full half maximum width approximately of the same size as the central peak of the solitons now are placed into a square lattice arrangement. The forcing intensity distribution is shown in Fig. 3(b). In Fig. 3(a) examples of spontaneously forming feedback solitons, which evolve without external control, are shown. Due to a inhomogeneous spatial distribution of the LCLV's nonlinearity the spontaneous feedback solitons, which also experience mutual interactions, form only in the lower left area of the aperture in the example. The experimental result of the external control is shown in Fig. 3(c). Now feedback solitons form distributed over the entire aperture, while they arrange perfectly according to the square lattice induced by forcing. Dependent on the forcing strength—above or below the writing threshold for feedback solitons—the feedback solitons possess bistability or they are ignited by the forcing. In Fig. 3 the forcing strength is above the ignition threshold for feedback solitons. However, we also obtain similar results when the individual solitons possess bistable features.

If the controlled system is operated below the ignition threshold for the creation of feedback solitons, an additional

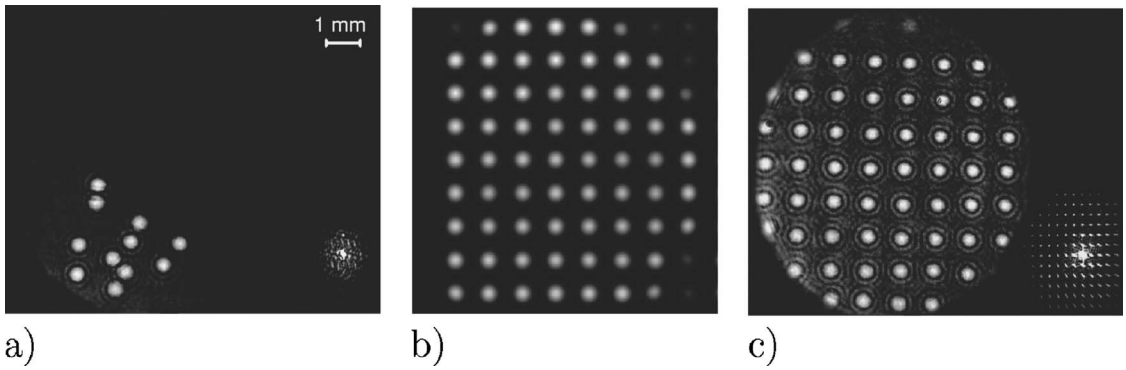

FIG. 3. Position control using an external incoherent amplitude control. (a) The uncontrolled system; the feedback solitons experience interaction and are located only in a small part of the aperture due to inhomogeneities. (b) The spatial distribution of the external control consists of a quadratic lattice with Gaussian shaped peaks at the lattice points. (c) The feedback solitons are positioned by the external control. The bottom right corner of the experimental images shows the far field (Fourier transform).

intensity distribution is required to ignite feedback solitons. If we use an additional uniform intensity distribution for switching on feedback solitons, the feedback solitons do not accumulate at the random trapping positions of the uncontrolled system,[29] but instead arrange according to the quadratic lattice defined by the external control. Thus, forcing enables us to control the lateral positions of optical feedback solitons in creating artificial trapping positions for the feedback solitons.

B. Robust incoherent addressing

Apart from a spatial position control, a complete and robust addressing scheme for feedback solitons is a necessity for implementing all optical memories. In the following, we will demonstrate such a robust addressing scheme using an incoherent external amplitude control. Particularly, we will show that erasure of individual feedback solitons is rendered possible with incoherent signals. Previously, the erasure of feedback solitons has only been demonstrated with a coherent beam, which was π out of phase with the feedback wave I_w in the LCLV single feedback system.[24] In comparison to coherent schemes, incoherent schemes, which already have been implemented in other systems,[47,48] allow for a robust addressing, which is not influenced by interference or vibrations of the setup. Moreover, the light pulse does not need to originate from the same laser source as the optical pump of the feedback system. For the purpose of implementing the incoherent addressing scheme, we operate the single feedback system at a pump intensity I_p slightly below the existence of bistability. If a small forcing intensity distribution is added, the forcing shifts the existence of bistability towards the operating point originally outside the existence of bistability and thus the local presence of I_F enables the formation of bistable feedback solitons. However an additional local ignition light pulse is required for the creation of a feedback soliton. The system can be interpreted as the realization of an all-optical logical AND in this situation because both the static bias of the forcing intensity and another switching light pulse are needed for the creation of a feedback solitons. Instead of adding an independent ignition pulse from another source, also locally increasing the forcing intensity I_f can be used to ignite a feedback soliton. In experiment a duration of $\Delta t=1$ s has been chosen for the writing pulse. If the intensity of the forcing is locally turned off completely (duration in experiment again $\Delta t=1$ s), the feedback soliton is erased. This complete addressing scheme is more robust than a method based on destructive interference and thus can experimentally be implemented more easily. The experimental results of this complete addressing scheme are shown in Figs. 4 and 5.

Figure 4 shows the spatial distribution of the addressing. In the top row the spatial intensity distribution of the external control is depicted; the bottom row shows the system response in the feedback intensity I_w. At $t=0$ s the external position control is activated, but feedback solitons have not yet been addressed. At $t=3$ s four feedback solitons have been addressed in a diagonal line. The ignition signal of the upmost feedback soliton is visible in the intensity distribution of forcing. After writing feedback solitons along the diagonal, the forcing intensity was sequentially set to zero at the addressing positions in the addressing sequence. Thus, feedback solitons are erased. Finally, at $t=9$ s the external control is reset to the initial state. Apparently, the method of erasure functions well except for one feedback soliton positioned in the lower left corner. At this position a spatial inhomogeneity of the setup obstructs the erasure of the feedback soliton. These spatial inhomogeneities can be compensated by an additional external forcing signal as we have already demonstrated in Ref. 40. Note, that the addition of a forcing intensity contra-intuitively first results in a decrease of the feedback intensity I_w. The decrease in intensity, if small forcing intensity is added, results from a small negative slope of the dark uniform branch observed in an experimental measurement of the bistability hysteresis. Likely reasons for this decrease are either a small initial ellipticity of the incident optical beam caused by imperfect polarizing elements in front of the LCLV or a small asymmetry between the incident linear polarization state optical axis of the LCLV and the polarizer placed inside the feedback arm. Thus the dark positions in Fig. 4 indicate positions illuminated with a

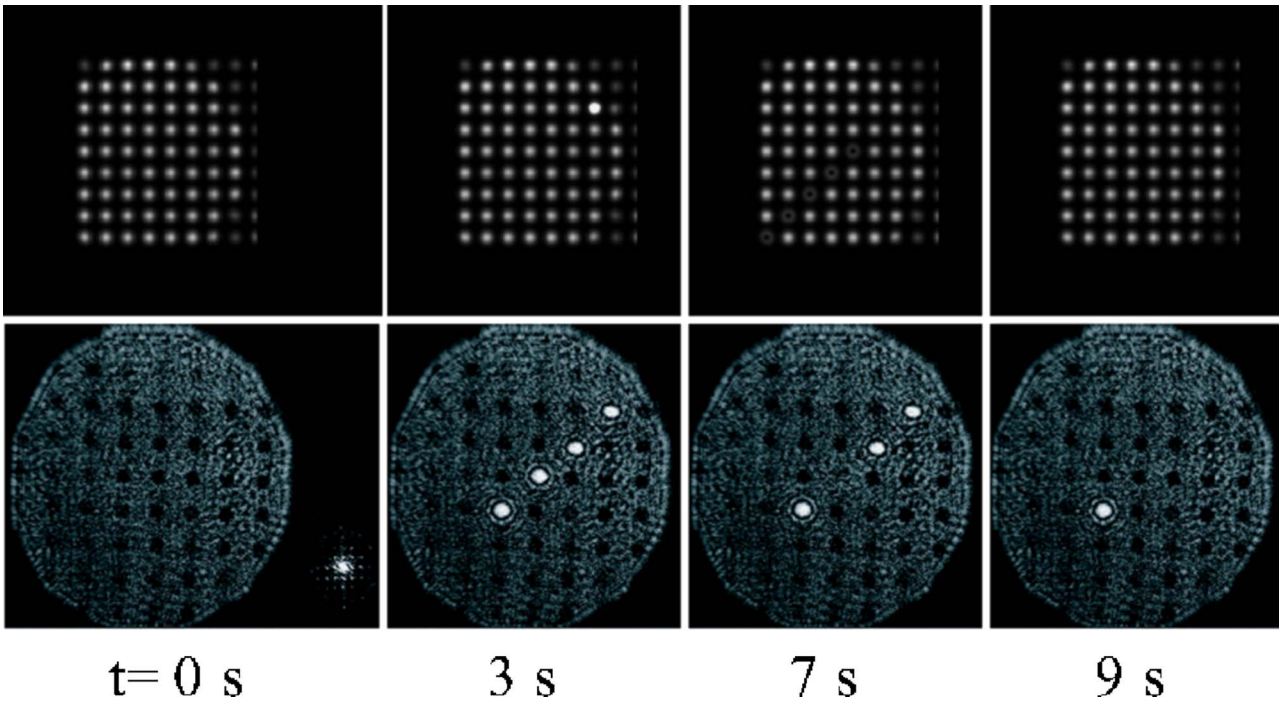

FIG. 4. (Color online) Images of a sequence with a complete addressing scheme. Top: signal of the external amplitude control. Bottom: write intensity I_w of the LCLV feedback system. A detailed description can be found in the text.

small forcing strength. At higher forcing intensities, the dark positions also become bright before a feedback soliton switches to the "on" state.

In order to demonstrate the reliability of the writing and erasure process, the temporal evolution of a repeated addressing scheme at a single addressing position is shown in Fig. 5. The diagram shows the local intensity of the feedback system I_w (line) as well as the temporal evolution of the local forcing signal (dashed line). The forcing intensity is increased from addressing cycle to addressing cycle. As expected, the system returns to the intensity value of the feedback soliton solution independently from the strength of the ignition pulse as soon as the addressing pulse exceeds the ignition threshold. Due to the restricted temporal resolution of the CCD camera (60 Hz), the previously investigated effect of critical slowing down[25] has not been observed in this experiment. The measurement however explicitly shows evidence that individual feedback solitons can be repeatedly written and erased in a robust manner by the incoherent addressing method. Thus we have demonstrated a previously inaccessible complete and robust addressing scheme for the LCLV system.

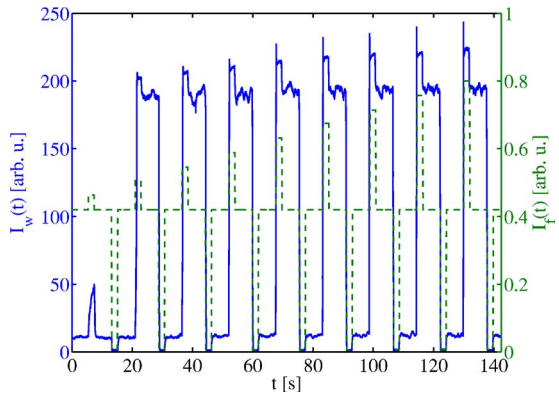

FIG. 5. (Color online) Intensity vs time plot of a repeated complete addressing scheme. The intensity of the external amplitude control in arbitrary units (line). The intensity of a single addressing position (dashed line). The maximum temporal resolution of the CCD camera is 60 Hz.

C. Gradient-dependent drift velocity

In the experiments described above the response of feedback solitons to external amplitude control was investigated by observing the final equilibrium state. However, to fully understand the influence of external amplitude control on the feedback solitons also soliton motions, which are induced by static amplitude control must be considered. In the following we will investigate and answer the question how feedback solitons respond to external amplitude forcing, if they are ignited laterally shifted with respect to a local extremum of the amplitude forcing. As a forcing signal we choose a cone shaped intensity distribution with maximum forcing intensity at the top of the cone, because a cone shape combines a cylinder symmetry with a linear gradient, which points towards the cone maximum from every direction. A three-dimensional image of such a cone-intensity distribution is shown in Fig. 6. In agreement with theory,[34] we expect the feedback soliton to move towards the maximum of the cone intensity, because amplitude forcing via the nonlinearity creates a corresponding extremum in the phase gradient of the feedback wave. In Fig. 7 the trace of the induced soliton motion is depicted in a magnified section of the aperture. Within the figure, positions of the feedback soliton are denoted by circles (○). The feedback soliton is ignited at the

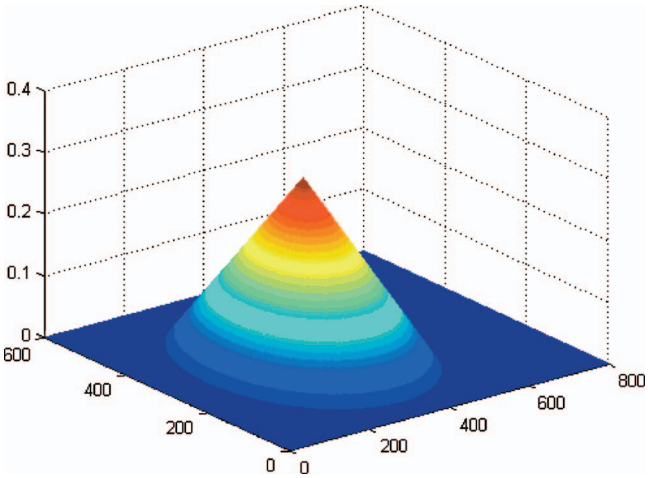

FIG. 6. (Color) Intensity profile of the cone used as external amplitude control for the investigation of gradient dependent drift velocities.

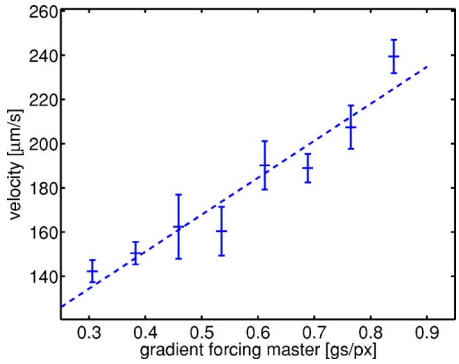

FIG. 8. (Color online) Averaged velocity of a feedback soliton vs variable intensity gradient. For each data point an average over five measurements has been taken. The error bars are the standard deviation of the data points. The gradient is measured in gray scale (gs) per pixel (px) of the forcing master. The dashed line is a guide to the eye.

right and moves towards the left. From its starting position to the end position the soliton moves approximately a distance of two and a half times the central soliton peak diameter. The background depicts an inverted gray scale image of the system response to the cone-shaped forcing without a feedback soliton. The arrows show the gradient in the intensity distribution I_w, which can be of used as a rough indicator for the induced phase gradient. Note however that the intensity distribution I_w cannot be assumed to linearly map the phase shift induced at the LCLV by the cone-shaped forcing intensity distribution, as the phase modulated wave experiences free space propagation and passes the polarizer (P01) on its path. To gain an exact measure of the induced phase it was required to use the expressions (1) and (2), however this still would not account for spatial inhomogeneities of the LCLV, which are mainly responsible for the variations observed in I_w. Thus even though I_w must be assumed to be an imperfect indicator for the phase shift ϕ_F induced by the forcing I_F, it is the best experimental measure available. As the feedback soliton cannot be assumed as point-like object, the average over the central peak area of the feedback soliton has been considered for the determination of the gradient in the intensity distribution I_w. The soliton trajectory indeed shows, that the feedback soliton moves towards the position of the maximal intensity of the cone-shaped forcing. Slight variations in the track can be explained by local inhomogeneities of the induced gradient.

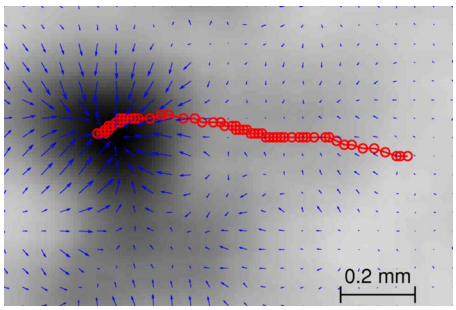

FIG. 7. (Color online) Motion of a feedback soliton at a cone-shaped intensity gradient. The background depicts the system response to the cone gradient without a feedback soliton (inverted gray scale). The trajectory of the feedback soliton, which moves from right to left, is denoted by ○. Additionally the local gradients are marked with arrows.

In the following, the influence of the strength of the gradient is investigated. For this purpose the inclination angle of the cone distribution has been increased, while the maximal intensity of the top of the cone remained fixed. To investigate the soliton motion the averaged velocity of the feedback solitons has been determined. In Fig. 8 the average velocity of the solitons measured in microns per second (μm/s) has been plotted against the absolute value of the increasing cone gradient measured in gray scales per pixel (gs/px) of the forcing master. Each data point of the graph contains the average of five independent measurements. The error bars in the plot denote the standard deviation for the averaged data points. Thus, as a reasonable estimate of the error of each data point the maximum sized error bar can be assumed. In the graph the average velocity of feedback solitons rises with higher values of the cone gradient. The relation between cone gradient and averaged velocity roughly appears to be linear, thus confirming the theoretical prediction of a linear relation between drift velocity of a soliton and local phase gradient.[34,35] The dashed line in the graph serves as a guide to the eye.

In Fig. 9 the instantaneous local velocity along the trajectory (+) of an exemplary measurement is plotted against time. The instantaneous velocity shows an interesting time dependence. At the starting point of the sequence ($t \approx 2.5$ s) and again around $t \approx 4.5$ s, two distinguished peaks are observed in the evolution of the instantaneous velocity. At times larger than approximately $t \approx 6$ s the feedback soliton has reached its final position. The fluctuations in the velocity profile at this time can be taken as a good estimate for the minimum error in the instantaneous velocity measurement.

In the same figure also the absolute value of the local gradient is plotted (*) in arbitrary units. Similar to the graph of the instantaneous velocity two peaks ($t \approx 2.5$ s and $t \approx 5$ s) are observed in the absolute value of the local gradient. The positions of both peaks in instantaneous velocity and local gradient coincide quite well, while the relative height of the peaks differs. The principal variations in rela-

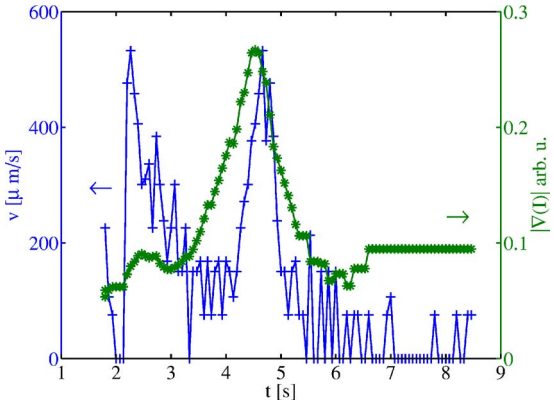

FIG. 9. (Color online) Position-dependent velocity (+) of a single feedback soliton moving at a cone gradient and absolute value of the local gradient (*).

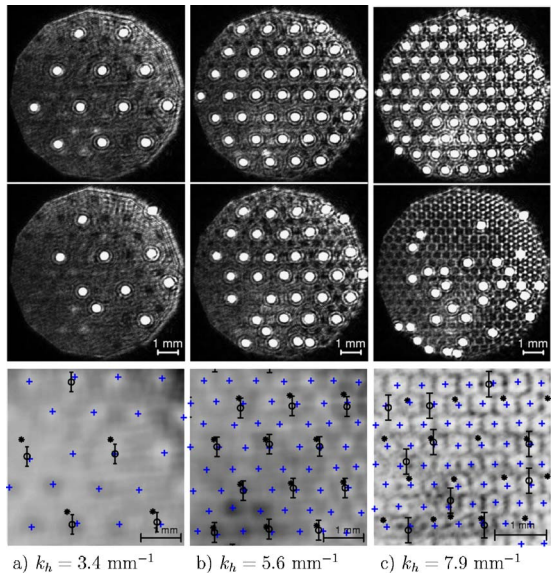

FIG. 10. (Color online) Feedback soliton motion in an hexagonally shaped gradient. Measurements at different wave numbers k_h of the forcing hexagon. (a) k_h=3.4 mm^{-1}. (b) k_h=5.6 mm^{-1}. (c) k_h=7.9 mm^{-1}. Top row: addressing of feedback solitons. Center row: final equilibrium state. Bottom: inverted gray scale image of the pure hexagonal gradient with indication for the addressing position (*), the final equilibrium position (○), and the local extrema of the hexagonal grid (+).

tive peak height are typical for our measurements of instantaneous velocity and local gradient, which have been performed at different addressing positions and varying gradient slope with several repetitions. Even though the relative peak heights vary from measurement to measurement the peak positions observed in the plots of instantaneous velocity and local gradient coincide in our measurements.

Several reasons for these imperfect matches of the relative peak heights need to be considered. For times $t \gtrsim 6$ s the feedback soliton already has reached its final equilibrium position. A close up observation of the data plotted in Fig. 7 however reveals that a small deviation between the position of the cone maximum and the final position of the feedback soliton exists. This deviation is much smaller than the diameter of the soliton peak. The differences between the relative height of local gradient and instantaneous velocity for times larger than $t \approx 6$ s thus are explained. More important are the relative peak height differences at $t \approx 2.5$ s and $t \approx 5$ s observed in the exemplary selected plot of instantaneous velocity and local gradient (Fig. 9). Apart from noise causing these fluctuations in relative gradient and instantaneous velocity heights we also need to consider that the response of the feedback system monitored in the feedback intensity I_w cannot be assumed to linearly map the phase distribution ϕ_F induced by the forcing intensity I_F. Free space propagation occurring in front of the detection which causes self-diffraction of the beam as well as the polarizing element (P) placed inside the feedback loop obstruct this linear mapping of feedback intensity I_w to the induced phase shift ϕ_F.

Note however that for the measurement of the averaged velocities plotted in Fig. 8 the variation of the forcing master and not the variation present in I_w has been accounted for. Therefore in this case the values of the varying gradient are not influenced by experimental imperfections.

Furthermore, the local variations of the velocity with respect to the local gradient could also be explained by an interaction between the cone gradient and the ring structure of the feedback solitons, which is known to possess a large influence onto the mutual soliton interactions.[29,49] Qualitatively, from the coincidence of the peak positions observed in different measurements of instantaneous velocity and local gradient, we however assume the influence of the interaction between the ring structure and the cone gradient to be small in comparison to the influence of the local inhomogeneities of the gradient. In some cases we have however observed, that superposition of the ring structure with the cone peak may lead to the ignition of a feedback soliton, which in the following interacts with the previously existing feedback soliton in the known manner.

A clear quantitative identification of the different effects contributing to the differences in the relative peak height between local gradient and instantaneous velocity however yet remains open. Nonetheless, we have thus clearly found a qualitative correlation between instantaneous velocity of feedback solitons and local gradients, which appears in their relative peak positions and more importantly a linear relation between averaged velocities and gradient of the forcing master was demonstrated quantitatively in this section.

D. Motion of feedback solitons in periodically structured gradients

After studying the influence of a rather simple gradient on the motion and position of feedback solitons, now the influence of external intensity control with spatially more complex intensity distributions will be investigated. As forcing, hexagonal intensity distributions with altering hexagon wavelengths have been used (see Fig. 10). Also compare to Ref. 44. Experiments were performed at hexagon wave numbers k_h between k_h=3.4 mm^{-1} [Fig. 10(a)] and k_h =7.9 mm^{-1} [Fig. 10(c)]. As before feedback solitons were written laterally shifted with respect to the maximum of the hexagonal gradient. Every second maximum of the hexagon control lattice has been chosen as an addressing position and the feedback solitons were addressed laterally shifted by 1/3 of the hexagon wavelength at an angle of −30° with respect

to the y-axis [the addressing positions are denoted as (∗) in the bottom row of Fig. 10]. After $t=1$ s of addressing, only the hexagonal gradient remains as forcing and the feedback solitons are free to interact with the hexagonal forcing lattice. Exemplary images of the interaction are shown in Fig. 10. The top row of the figure depicts the moment of writing feedback solitons, while the row in the center shows the final equilibrium state after interaction with the control lattice. In the bottom row, on top of an enlarged image of the hexagonal forcing lattice in inverted gray scale, the addressing positions (∗), the final equilibrium position (○) of the feedback solitons as well as the local extrema of the hexagonal forcing grid (+) are indicated. The error bars at the final equilibrium position (○) denote the averaged diameter of the central soliton peaks.

From the images of the addressing and of the final equilibrium state it can be qualitatively deduced, that in the measurements at $k_h=3.4$ mm^{-1} and $k_h=5.6$ mm^{-1} the feedback solitons are on average trapped by the hexagonal forcing, because the final equilibrium state resembles the original addressing geometry, even though some of the ignited feedback solitons disappear. The measurement at $k_h=7.9$ mm^{-1} (right column) appears to become disordered. The disorder also is observed in the dynamics preceding the final equilibrium. In contrast to the sequences with smaller wave numbers, for $k_h=7.9$ mm^{-1} interactions between neighboring feedback solitons and increased spontaneous motions are observed. In order to gain a more quantitative measure of the quality of trapping to the hexagonal grid we have analyzed the measured data in two approaches using a measurement of absolute positions as well as a Fourier method.

In the first approach the measurement of the final equilibrium positions of the feedback solitons and of the local extrema of the hexagonal forcing are used. From these measurements averaged minimal distance $d_{\min}$ between the final equilibrium positions of the feedback solitons and the next neighbor position of the local extremum was calculated. To gain a measure of the quality of the hexagon trapping q_R the averaged minimal distance $d_m in$ has been scaled to the wavelength of the hexagonal forcing Λ_h to make q_R independent of the hexagon scaling. We define the measure for quality of trapping derived from the analysis of real space as

$$q_R = \frac{\Lambda_h}{d_{\min}}. \tag{4}$$

Finally we normalize the maximum value of the quality factor of trapping q_R to unity. The quality factor q_R is plotted (○) in Fig. 11. As can be seen in the graph the quality of trapping q_R remains at a saturation level up to the measurement of $k_h=5.6$ mm^{-1}. At higher wave numbers the quality factor q_R decreases indicating the loss of a trapping condition.

The second approach to derive a quality factor q of the trapping uses the Fourier transform of the spatial optical field. Exemplary images of the far field (Fourier transform of I_w) are depicted in Fig. 12. The images from left to right depict the optical Fourier transform of the system response I_w to (a) the pure hexagonal gradient $k_h=5.6$ mm^{-1} (b) at the moment of addressing (t_{add}) of optical feedback solitons (c)

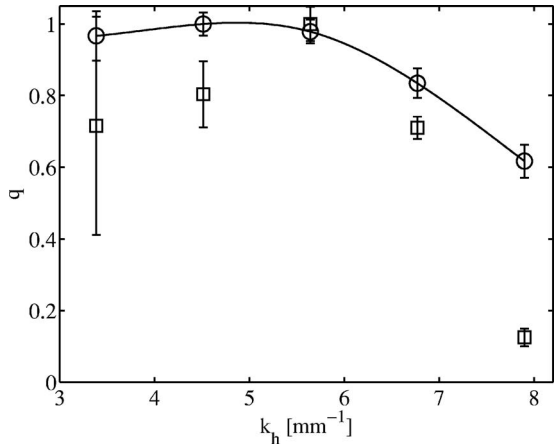

FIG. 11. Plot of the quality of trapping q_R (○), q_F (□) induced by the hexagonal forcing against the wave number $k_h=5.6$ mm^{-1} of forcing. q_R has been determined from absolute distances in real space, while q_F is derived from a Fourier analysis. The line is a mere guide to the eye.

the final equilibrium state (t_{eq}). For the derivation of the quality factor q_F the Fourier modes marked in (b) have been selected. We calculate q_F according to

$$q_F = \frac{I_g(t_{\text{add}})}{I_\square(t_{\text{add}})}\frac{I_\square(t_{\text{eq}})}{I_g(t_{\text{eq}})}, \tag{5}$$

where $I_\square$ is the total intensity of the Fourier modes marked in Fig. 12 with a (□), and $I_g=I_\square+I_\bigcirc$, where $I_\bigcirc$ denotes the total intensity excited in the Fourier modes marked with a circle (○). The resulting quality factor q_F is also plotted against the wave number of the hexagonal gradient in Fig. 11. Comparison between both quality factors yields a qualitative agreement in curve progression. A maximum of trapping is observed at $k_h=5.6$ mm^{-1}; further increase of k_h results in a rapid decay of the quality factor q_F of trapping to the hexagonal grid. Different from the analysis of real space, which remains at a saturation level before it decreases, the quality factor q_F experiences a slight rise at $k_h=5.6$ mm^{-1}. The increase to this value likely results from the increasing number of feedback solitons, which contribute to the intensity distribution in Fourier space. It thus can be assumed to be a statistical effect.

The loss of a trapping condition at higher wave numbers observed in both methods of analysis can be explained by the decreasing distance between feedback solitons which allows

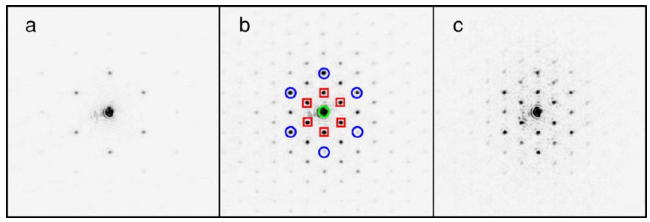

FIG. 12. (Color online) Optical Fourier transform of the center column of Fig. 10 (wave number hexagon forcing: $k_h=5.6$ mm^{-1}). (a) Hexagonal gradient only; (b) addressing of optical feedback solitons. The markers indicate the Fourier modes, which are selected for analyzing the system state. For details of the analysis, please refer to the text. (c) Final equilibrium state. The images depict an inverted gray scale.

for mutual interaction of neighboring feedback solitons, thus disturbing the trapping. The motion of cavity solitons in periodically structured phase gradients has also been investigated theoretically.[32,33] A reversion of their direction of motion from attraction to the maximum of the phase gradient to attraction to the minimum is reported, if the modulation period of the gradient undergoes a certain threshold value. Even though we have not observed a representative locking to off site positions in the measurement at $k_h=7.9\ \mathrm{mm}^{-1}$, some feedback solitons are however observed which position themselves in between two hexagon maxima. Note that this effect has not at all been observed in measurements at other wave numbers. Compare this value, which characterizes the minimal achievable by the forcing induced position control with the wave number corresponding to the peak soliton diameter $k_S=17.3\ \mathrm{mm}^{-1}$ and with the wave number corresponding to the diameter of the first order self-diffraction ring $k_R=10\ \mathrm{mm}^{-1}$. At the hexagon wave number $k_h=8-9\ \mathrm{mm}^{-1}$ one can therefore assume that the feedback soliton including its oscillating tails already covers more than just one maximum of the hexagon gradient and thus for the motion of the soliton an average over the covered area needs to be considered.

Besides the strength of the gradient, a periodicity of the gradient also influences the motion of optical feedback solitons. In our experiment we observe trapping to a hexagonally shaped gradient below a hexagon wave number of $k_h=7\ \mathrm{mm}^{-1}$. Optimal trapping occurs around $k_h=6\ \mathrm{mm}^{-1}$. If we briefly reconsider the situation of the experiment with the cone gradient (cf. Fig. 7), we can conclude from the experiment with the periodically structured hexagon gradient, that also the wavelength of small inhomogeneities has to be taken into account for the motion at the cone gradient. Particularly inhomogeneities will also influence the deviations from the optimal path dependent on their wavelength.

E. Dynamic positioning

In previous sections the static and dynamic response of optical feedback solitons to static external control has been investigated. It was demonstrated that gradients induced by the forcing serve for the lateral positioning and trapping of feedback solitons. The static forcing also succeeds in inducing motions if the gradient induced by the static control is in vicinity of the soliton positions. A movement over larger distances however cannot be achieved in the way described, because higher forcing intensities, which are required for the inducing of long range motions, would lead to ignition of additional feedback solitons. The alternative however is to move the forcing gradient itself. In the following we will thus extend the static external control method to a dynamic forcing scheme. For this purpose, movies with dynamic intensity distributions are applied instead of forcing signals with static intensity distributions. In the following, a chessboard pattern is used as forcing intensity distribution, which slides from right to the left in the dynamic forcing sequence. An exemplary sequence of the induced motion is shown in Fig. 13.

The sequence shows only a section of the aperture. The time interval between the images is $\Delta t=6.7$ s. Note that feedback solitons ignite near to the right margin of the aperture, because the forcing intensity in this region is operated slightly above the ignition threshold for feedback solitons. After ignition the feedback solitons drift towards the left and thus shift their position according to the motion of the forcing movie. The sharp border of the chessboard compartments which induces a steep local gradient is therefore responsible for the soliton movement, as it pushes the feedback solitons towards the left. Two lines of reference are added to the sequence to illustrate the motion of the feedback solitons and of the forcing.

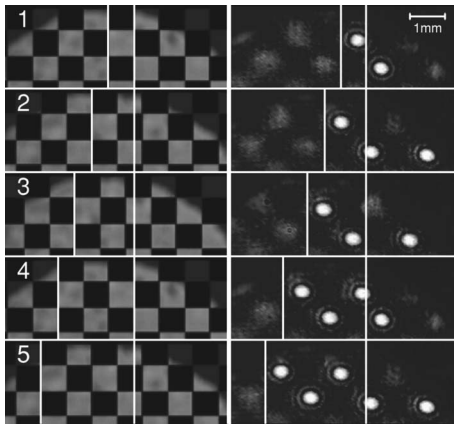

FIG. 13. Sequence with dynamic positioning of optical feedback solitons. A section of the aperture is shown. Left column: signal of the forcing movie. Right column: the response of the feedback solitons. The feedback solitons ignite at the right, while the forcing input, which consists of a chessboard pattern, moves to the left. The feedback solitons follow the motion of the forcing input. The reference lines illustrate the movement. The time interval between the images is $\Delta t=6.7$ s.

Yet, the dynamic positioning has been demonstrated in a comparatively small area of the beam aperture. In other sections we have observed erasure of feedback, brief sticking of feedback solitons to spontaneous pinning positions, and spontaneous interactions between feedback solitons. The effects however are not a principle obstacle and can be suppressed if the intensity of forcing strength is locally more carefully adjusted with respect to the pump intensity as an intention of compensating for spatial system inhomogeneities.[40]

Nonetheless, the experiments demonstrate the powerful capability of forcing to move and reposition individual localized structures in a yet unknown way. The dynamic motion, which we have demonstrated here can for example be useful for the implementation of a shift register for optical feedback solitons.

IV. CONCLUSIONS AND OUTLOOK

In conclusion, we have experimentally demonstrated, that external amplitude control is a powerful tool for dynamic and static control of optical feedback solitons. An optical single feedback experiment with a LCLV as nonlinearity has been chosen as a model system for the demonstration of different novel techniques implementing two-dimensional dynamic amplitude and phase control. External amplitude control allows for the static position control of optical feed-

back solitons. Without control, the behavior of feedback solitons is dominated by spontaneous motions and interactions. External amplitude control succeeds in arranging the feedback solitons in accordance with predefined control lattices of principle arbitrary geometry.

If the control strength is adjusted appropriately we have demonstrated that external amplitude control allows for the implementation of an incoherent, complete, and robust addressing scheme for optical feedback solitons, which previously required coherent and less robust schemes especially for the erasure of feedback solitons in the LCLV experiment. Furthermore, the experimental investigations on the response of feedback solitons to induced gradients confirms the robustness of the control method against lateral perturbation of the soliton position as well as it confirms theoretical predictions on the motion of optical feedback solitons in a system with a large aspect ratio.

In experiments using a cone-shaped gradient we have extended the investigations to the experimental analysis of the control induced motions of feedback solitons. The linear gradient pointing from every direction to the center of the cone is excellently suited to investigated the dependence of the drift velocities of feedback solitons on the gradient steepness experimentally. Both the experimental measurement of averaged velocities against steeper gradients and the experimental measurement of the instantaneous velocities in comparison to the local gradient at least qualitatively confirm the theoretical prediction of a linear relation between the drift velocities of feedback solitons and the slope of a parameter gradient.[34,35] In case of the measurement of average velocities with respect to the increasing gradient slope where the cone slope of the forcing master was changed even confirms this relation quantitatively. These experiments also demonstrate the usefulness of the external amplitude control for the creation of artificial trapping positions for feedback solitons, which control their lateral positions. The experiment also confirms the robustness of the position control against perturbations. If a feedback soliton laterally shifts spontaneously, the attractive force to the local forcing maximum demonstrated in the cone experiment will re-establish the positioning initially intended by a potential user.

Investigating the motion of feedback solitons in a hexagonal gradient we observe a dependence of the trapping properties of the gradient on the wavelength of the hexagonal control lattice. Trapping to the hexagon forcing is lost above a hexagon wave number of $k_h \approx 7\ \mathrm{mm}^{-1}$. Even though inhomogeneities and soliton interactions challenge the experimental investigations, nevertheless, indications of potential reversed soliton motion, where the solitons dependent on the wavelength of a periodic phase gradient accumulate at the minima of the gradient have been observed.[32] Finally, the realization of a dynamic control scheme allowing for the dynamic repositioning of feedback solitons has successfully been demonstrated. The dynamic forcing scheme can be utilized to redistribute feedback solitons once they have been switched on and the method can thus be utilized for the implementation of an all optical shift register. Although the methods presented in this article have exemplary been investigated at the LCLV single feedback system as a model system, they have definitely more far-reaching implications. The principles are of utmost relevance for many other optical systems, which exhibit formation of optical dissipative solitons. Particularly, our methods can be useful for an implementation of control in active or passively driven nonlinear optical resonators.

[1] M. Segev, B. Crosignani, A. Yariv, and B. Fischer, Phys. Rev. Lett. **68**, 923 (1992).
[2] C. Denz, W. Krolikowski, J. Petter, C. Weilnau, T. Tschudi, M. R. Belic, F. Kaiser, and A. Stepken, Phys. Rev. E **60**, 6222 (1999).
[3] M. Peccianti and G. Assanto, Opt. Lett. **26**, 1690 (2001).
[4] M. Warengham, J. Henninot, and G. Abbate, Opt. Express **2**, 483 (1998).
[5] *Dissipative Solitons*, edited by N. Akhmediev and A. Ankiewicz (Springer, Berlin, 2005).
[6] D. W. McLaughlin, J. V. Moloney, and A. C. Newell, Phys. Rev. Lett. **54**, 681 (1985).
[7] G. S. McDonald and W. J. Firth, J. Mod. Opt. **37**, 613 (1990).
[8] W. Firth and A. Scroggie, Phys. Rev. Lett. **76**, 1623 (1996).
[9] C. Etrich, U. Peschel, and F. Lederer, Phys. Rev. Lett. **79**, 2454 (1997).
[10] W. J. Firth and G. K. Harkness, Asian J. Phys. **7**, 665 (1998).
[11] M. Brambrilla, L. Lugiato, F. Prati, L. Spinelli, and W. Firth, Phys. Rev. Lett. **79**, 2042 (1997).
[12] V. Taranenko, K. Staliunas, and C. Weiss, Phys. Rev. A **56**, 1582 (1997).
[13] D. W. McLaughlin, J. V. Moloney, and A. C. Newell, Phys. Rev. Lett. **51**, 75 (1983).
[14] M. Tlidi, P. Mandel, and R. Lefever, Phys. Rev. Lett. **73**, 640 (1994).
[15] N. N. Rosanov and G. V. Khodova, J. Opt. Soc. Am. B **7**, 1057 (1990).
[16] Y. I. Balkarei, M. G. Evtikhov, J. V. Moloney, and Y. A. Rzhanov, J. Opt. Soc. Am. B **7**, 1298 (1990).
[17] G. S. McDonald and W. J. Firth, J. Opt. Soc. Am. B **7**, 1328 (1990).
[18] W. Firth, J. Mod. Opt. **37**, 151 (1990).
[19] E. Ciaramella, M. Tamburrini, and E. Santamato, Appl. Phys. Lett. **63**, 1604 (1993).
[20] R. Neubecker, G.-L. Oppo, B. Thüring, and T. Tschudi, Phys. Rev. A **52**, 791 (1995).
[21] F. Arecchi, S. Boccaletti, S. Ducci, E. Pampaloni, P. Ramazza, and S. Residori, J. Nonlinear Opt. Phys. Mater. **9**, 183 (2000).
[22] T. Ackemann and W. Lange, Appl. Phys. B **72**, 21 (2001).
[23] B. Schäpers, T. Ackemann, and W. Lange, J. Opt. Soc. Am. B **19**, 707 (2002).
[24] M. Kreuzer, B. Thüring, and T. Tschudi, Asian J. Phys. **7**, 678 (1999).
[25] A. Schreiber, B. Thüring, and M. Kreuzer, Opt. Commun. **136**, 415 (1997).
[26] P. Ramazza, S. Ducci, S. Boccaletti, and F. Arecchi, J. Opt. B: Quantum Semiclassical Opt. **2**, 399 (2000).
[27] W. J. Firth and C. O. Weiss, Opt. Photonics News **2002**, 54 (2002).
[28] W. J. Firth and A. J. Scroggie, Phys. Rev. Lett. **76**, 1623 (1996).
[29] B. Gütlich, R. Neubecker, M. Kreuzer, and T. Tschudi, Chaos **13**, 239 (2003).
[30] A. G. Vladimirov, J. M. McSloy, D. V. Skryabin, and W. J. Firth, Phys. Rev. E **65**, 046606 (2002).
[31] M. Tlidi, A. G. Vladimirov, and P. Mandel, J. Propul. Power **39**, 216 (2003).
[32] A. J. Scroggie, J. Jeffers, G. McCartney, and G.-L. Oppo, Phys. Rev. E **71**, 046602 (2005).
[33] A. J. Scroggie, J. Jeffers, G. McCartney, and G.-L. Oppo, Phys. Rev. A **72**, 023824 (2005).
[34] T. Maggipinto, M. Brambilla, G. K. Harkness, and W. J. Firth, Phys. Rev. E **62**, 8726 (2000).
[35] U. Bortolozzo, P. L. Ramazza, and S. Boccaletti, Chaos **15**, 013501 (2005).
[36] G. Schliecker and R. Neubecker, Phys. Rev. E **61**, R997 (2000).
[37] P. L. Ramazza, S. Boccaletti, U. Bortolozzo, and F. T. Arecchi, Chaos **13**, 335 (2003).
[38] P. Ramazza, E. Benkler, U. Bortolozzo, S. Boccaletti, S. Ducci, and F. Arecchi, Phys. Rev. E **65**, 066204 (2002).
[39] B. Gütlich, M. Kreuzer, R. Neubecker, and T. Tschudi, Mol. Cryst. Liq. Cryst. Suppl. Ser. **375**, 281 (2002).
[40] B. Gütlich, H. Zimmermann, C. Denz, R. Neubecker, M. Kreuzer, and T. Tschudi, Appl. Phys. B **81**, 927 (2005).
[41] B. Schäpers, T. Ackemann, and W. Lange, Proc. SPIE **4271**, 130 (2001).
[42] N. N. Rosanov, Prog. Opt. **35**, 1 (1996).

[43]U. Bortolozzo and S. Residori, Phys. Rev. Lett. **96**, 037801 (2006).
[44]F. Pedaci, P. Genevet, S. Barland, M. Giudici, and J. R. Tredicce, Appl. Phys. Lett. **89**, 221111 (2006).
[45]R. Neubecker and A. Zimmermann, Phys. Rev. E **65**, 035205 (2002).
[46]R. Neubecker and O. Jakoby, Phys. Rev. E **67**, 066221 (2003).
[47]B. Schäpers, M. Feldmann, T. Ackemann, and W. Lange, Phys. Rev. Lett. **85**, 748 (2000).
[48]V. B. Taranenko and C. O. Weiss, Appl. Phys. B **72**, 893 (2001).
[49]P. Ramazza, U. Bortolozzo, S. Boccaletti, and F. Arecchi, Appl. Phys. B **81**, 921 (2005).